Facile Control of Corncobs-based Carbons with Eutectic Salt $ZnCl_2$/NaCl Templated for the Adsorption of Organic Aldehyde

Honglei Chen, Lei Sha, Yujie Zhang, Yu Liu, Fangong Kong, and Xin Zhao *

Corncob, a renewable biomass waste, has been successfully explored as a low-cost crude carbon source to prepare controlled morphology, and result in higher value-added carbons through a $ZnCl_2$/NaCl treatment and direct pyrolysis process. The synthesis route is simple, green, and results in carbons with different morphology and porous structures by varying the ratio of the eutectic salt $ZnCl_2$/NaCl. Moreover, the adsorption capacities of different carbon materials for formaldehyde and butyraldehyde were tested further. It was demonstrated that NaCl and $ZnCl_2$ could be utilized as a mesopore template, and as a micropore activation agent for carbon materials, respectively. Although the mesopores can provide a fast diffusion channel, and the micropores can enhance adsorption ability, the specific surface area originating from the mesopores was proportional to the amount of butyraldehyde adsorption, and the specific surface area of the micropores was beneficial to the amount of formaldehyde adsorption taking place. The adsorption isotherms follow Langmuir and pseudo first-order kinetic modeling. Additionally, the whole process belongs to physical adsorption.

Keywords: Corncobs; Eutectic salt; Controlled morphology; Adsorption ability

State Key Laboratory of Biobased Material and Green Papermaking, Qilu University of Technology, Shandong Academy of Sciences, Jinan, Shandong, 250353, P.R. China;
** Corresponding author: zhaoxin_zixi@126.com (Xin Zhao)*

INTRODUCTION

Low molecular weight organic aldehydes in the atmosphere have been major pollutants for many years due to their strong, toxic effects on the eyes, skins, and respiratory tracks of human beings. Several strategies have been developed to remove organic aldehydes, such as oxidation, biotechnology, directly blow-off, and adsorption approach (Falco *et al.* 2018; Kante *et al.* 2019). The adsorption process removes low-concentration harmful substances that are difficult to separate by common methods (Han *et al.* 2019). It has the advantages of high purification efficiency, useful recyclability, obvious energy saving qualities, economy, and environmental protection (Kanta *et al.* 2019). Carbon materials, as promising adsorbents, remove organic aldehydes from the atmosphere due to their high surface area, hierarchical porous structure, and chemical inertness (Fuchs *et al.* 2016; Valentín-Reyes *et al.* 2019). In addition, biomass-derived carbon materials have been explored.

A number of biomass wastes, such as sawdust, *Euonymus japonicas* leaves, palm shell, and corncob have been used to prepare carbon materials (Zhu *et al.* 2015; Karnan *et al.* 2017; Yek *et al.* 2019; Zhao *et al.* 2019). As an agricultural waste, corncob is produced at high levels because corn is widely cultivated across the planet. The spongy cellular structure of corncob may be favorable to the formation of porosity, and its wide availability also serves as an abundant and inexpensive feedstock option for the preparation of carbon materials.

During the synthesis of carbon materials through direct carbonization, it is difficult to control the porous structures and dimensions. The ion thermal approach provides a facile, sustainable, and large-scale strategy for synthesizing carbon materials. As shown in pioneering experiments, carbon materials were prepared by carbonization ionic liquid mixed with eutectic inorganic salts at high temperature (800 °C to 1000 °C) under inert atmosphere (Fellinger *et al.* 2013). The compatibility of the organic and the inorganic molten salts facilitated the molecular mixing of the two phases throughout the decomposition and carbonization process of the organic materials. This leads to the nanoseparation of the inorganic salt and the final carbon. Zinc chloride ($ZnCl_2$) is one of the activating agents most widely used in the preparation of different carbon materials with a high carbon yield and surface area (Liu and Antonietti 2014). Potassium chloride (KCl) and sodium chloride (NaCl) are porogens for carbon materials, which result in the different porous structures (Ma *et al.* 2014). The combination of an activating agent with a porogens leads to a "one-stone-two-birds" situation of controlling pore structure and surface area. However, it has seldom been applied to the carbon preparation that occurs from biomass carbonization.

The present research proposes a simple approach for the use of the agricultural waste, corncob, to produce novel carbon materials. The morphology and porous structures of corncob-based carbon was tailored by a modification of the ratio of a eutectic salt $ZnCl_2$/NaCl solution and the carbonization temperature. The prepared corncob-based carbon, with its proposed method, was employed as an adsorbing material to remove selectively organic aldehydes, namely formaldehyde and butyraldehyde gas. Furthermore, the adsorption properties and influencing factors of carbon materials on organic aldehydes were systematically investigated. The adsorption thermodynamics and kinetics theory were further analyzed for its application on industrial wastewater and the air pollution of biomass-derived carbon.

EXPERIMENTAL

Preparation of Carbon Materials

The carbon samples were prepared as follows. The corncobs (Jinan farm, China) were triturated with the corncob powders passing through 60 mesh sieves. The material was boiled for 0.5 h. Finally, the material was dried. A series of eutectic salt solutions were developed by dissolving 70 g of $ZnCl_2$/NaCl (Sigma, Augusta, America) with a different mass ratio of 1:0, 2:1, 1:1, 1:2, and 0:1 in 200 mL deionized water, respectively. The processed corncob powders (10 g dry weight) were each impregnated in a eutectic salt solution for 4 h, and then dried at 100 °C. Once the solution was dried, all the samples were further carbonized at 900 °C under a nitrogen atmosphere. The prepared samples were denoted as C-Zn, C-2, C-1, C-0.5, and C-Na, respectively. For comparison, the control was produced from corncob powders via a direct carbonization at 900 °C under nitrogen atmosphere (denoted as carbon).

Characterization

Scanning electron microscopy (SEM) was performed using a JSM-7401F microscope (JEOL, Hokkaido, Japan) at an acceleration voltage of 20 kV. The images of the transmission electron microscopy (TEM) were obtained on a JEOL 2011 (JEOL, Hokkaido, Japan) apparatus that was operating at 200 kV. The sample was first dispersed in ethanol and then subjected to ultrasound. Further, the upper layer of liquid was taken out, and then ethanol was added, followed by a continuation of dispersing with ultrasound. After several dispersed-ultrasound process cycles, the supernatant solution was placed dropwise on the test copper mesh and dried at room temperature. Powder X-ray diffraction (XRD) patterns of the samples were measured using a Brucker D4 (Bruker, Frankfurt, Germany) powder X-ray diffractometer with Cu Kα radiation at 40 kV and 40 mA. Nitrogen sorption isotherms were measured with a Micromeritics ASAP 2020 sorptometer (Maike, Augusta, America) using nitrogen as the adsorbate at 77 K. All samples were degassed at 300 °C for more than 10 h before the analysis. The specific surface area (S_{BET}) was calculated using the NLDFT method based on the adsorption data in the relative pressure range of 0.05 to 0.2, and the total pore volume was determined at the highest relative pressure.

Adsorption Tests

The measurement of the adsorption capacity of organic aldehyde by Intelligent Gravimetric Analyzer (IGA, HIDEN company, UK) was carried out. The IGA contains a precise pressure, temperature control system, and an ultra-sensitive thermostatic balance with an accuracy of 0.1 μg. Firstly, the adsorbent sample was vacuumed to purify the substance at high temperature, and then the adsorption pressure point was set to slowly increase the pressure of the whole system through computer control. Meanwhile, the computer tracked and recorded the changes of adsorbent relative to time and weight, and the temperature control accuracy of the adsorbent was ±0.1 °C. The computer detects the rate of adsorption close to equilibrium and analyzes the data to ensure the accuracy of the data (Chen *et al.* 2012).

The procedure was continued out as follows: First, 10 mg samples were washed and removed from the water. The obtained samples were placed in the sample chamber under a temperature of 180 °C and a high vacuum setting ($<10^{-3}$ Pa) for 10 h, after which the temperature was cooled down to 25 °C. After the cooling step, formaldehyde and butyraldehyde gases of different pressures were added to the sample chamber and the adsorption equilibrium of the samples were tested at each pressure level. Finally, the adsorption isotherms of the organic aldehyde were obtained.

RESULTS AND DISCUSSION

All the samples showed different morphological features (Fig. 1). As can be observed in Fig. 1a, the corncob-derived carbon without a eutectic salt template displayed irregularity in its morphology from the decomposition of cellulose, hemicellulose, lignin and the structure of the corncob itself (Jiang *et al.* 2016). The C-Zn sample (Fig. 1b) appeared as a connected, reef-like structure. This kind of phenomenon may be due to the $ZnCl_2$ effect on the cellulose of biomass, where swelling, peptizing, and dissolving of the pores formed occurs. Additionally, the $ZnCl_2$ effect leads to a shrinkage of the macropores that takes place after the pores dissolve (Spagnoli *et al.* 2017). By adding the NaCl active agent, C-2 (Fig. 1c) shows a regularity of spheres that were about 2 μm on the reef. When the $ZnCl_2$/NaCl reached to 1, C-1(Fig. 1d) displays clear spherical structures, as well as further aggregation between the spheres. However, as can be seen in

Fig. 1c, it is interesting that the spheres gradually broke down. By contrast, C-0.5 (Fig. 1e) shows a cracked tube-like structure with a 4 μm width, as well as a large number of pores in the wall of the tube. However, the C-Na sample (Fig. 1f) shows macropores with larger holes at about 10 μm in diameter. This finding is attributed to the $ZnCl_2$'s ability to catalyze the conversion of the biomass derivatives via stripping away the hydrogen and oxygen atoms in the carbon source. Meanwhile, it is clear that the ratio of the eutectic salt $ZnCl_2$/NaCl has an obviously influence on the sample morphology. The $ZnCl_2$/NaCl catalyzes the conversion of the corncobs to the C=C and C=O containing compounds and then further carbonizes the compound to form the carbon materials rich in oxygen-containing groups (Kim and Jeon 2015). These interconnected macropores might be derived from the combination of inherent macropores in the cellular structures of the corn husks with different eutectic salt ratios. However, these morphologies will serve as reservoirs to adsorb the metal ions, and these thicker pore walls can provide a large amount of interface for the ion storage and adsorption (Hattori *et al.* 2017).

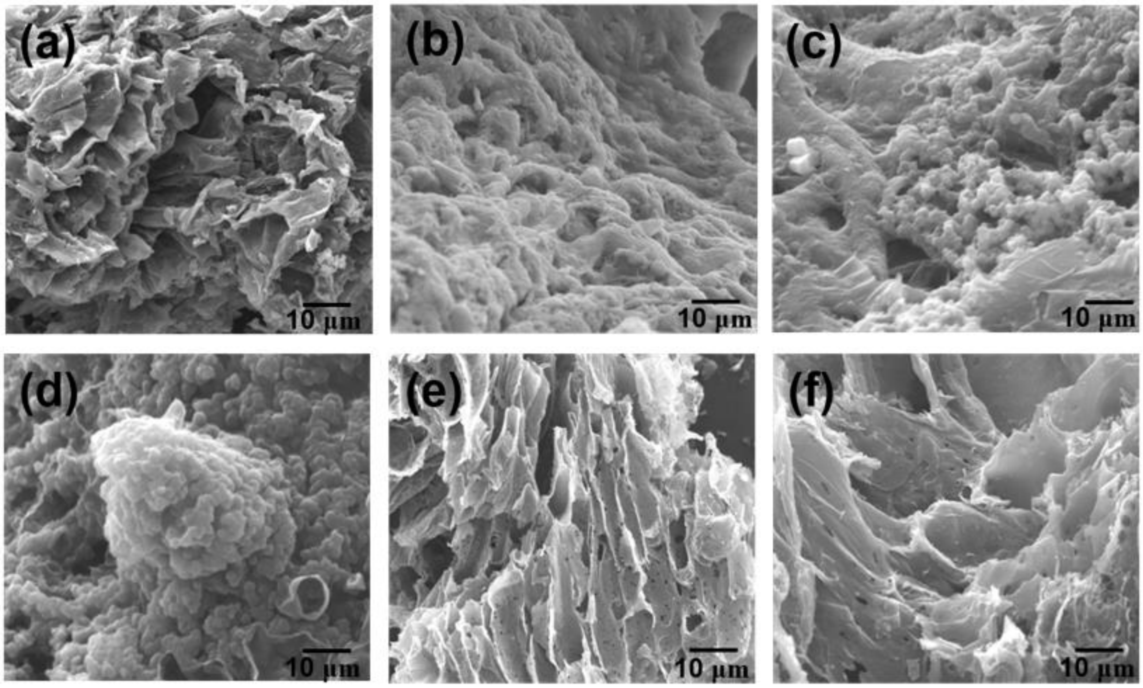

Fig. 1. SEM images of the different carbon samples (a, Carbon; b, C-Zn; c, C-2; d, C-1; e, C-0.5; f, C-Na)

The TEM images of the as-prepared carbon materials are shown in Fig. 2. Each of the samples displayed an intrinsic and special microstructure, as well as abundant porosity. The porous structures had slight changes from disordered crack-like pores on the control to ordered point-like pores on the C-Zn, to disordered worm-like pores on the C-2, C-1, and C-0.5, and to finally ordered to ripple-like pores of the C-Na. The results can be ascribed to the presence of mineral salts that affected the charring and aromatization of the corncob's molecular skeleton and led to the creation of diversiform porous structures (He *et al.* 2013). The carbon materials with the ordered pores were derived from corncob when a single salt ($ZnCl_2$ or NaCl) was used as the functional agent. The disordered worm-like pores were generated with the utilization of the eutectic salts ($ZnCl_2$ and NaCl), which may be ascribed to reciprocal inhibition from both of the salts. Nevertheless, these ordered or disordered porous structures provide a high surface area and adsorption ability for the prepared corncob-derived carbon materials.

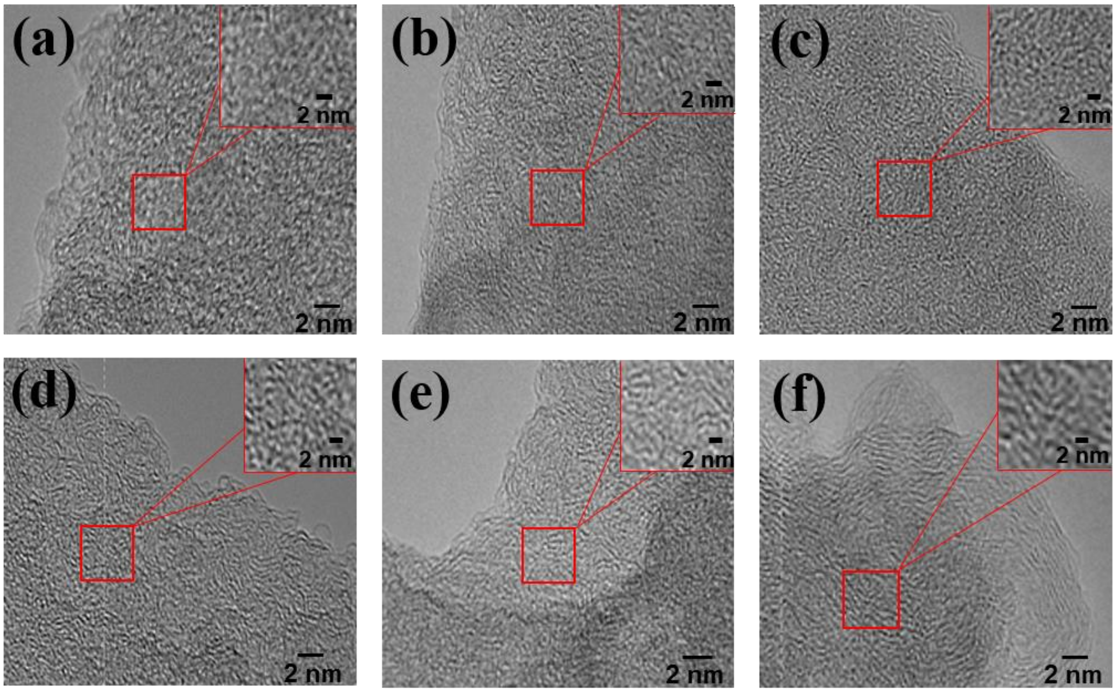

Fig. 2. TEM images of the different samples (a, Control; b, C- Zn; c, C-2; d, C-1; e, C-0.5; f, C-Na)

The XRD analysis showed that all the samples had similar XRD patterns. Two diffraction peaks appeared at 2θ of 23° and 44° with large widths and low intensities, which are the typical characteristic peaks of the graphitic carbon (Gao *et al.* 2014).

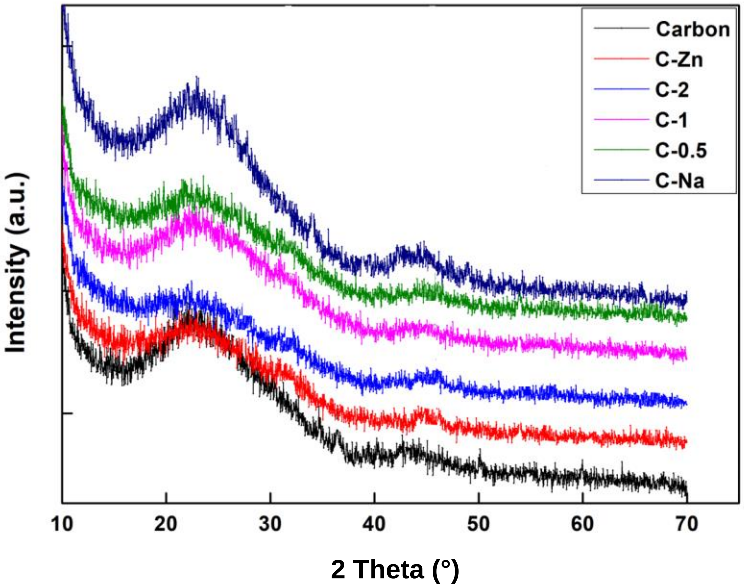

Fig. 3. XRD images of the different carbon samples

There were no obvious diffraction peaks resulting from the porogen salts in the XRD images. These findings indicate that only a trace amount of porogen salts were present in the as-prepared carbon materials. This suggests that residue from most of the salts were removed via evaporation and a washing that followed.

The nitrogen adsorption isotherms and the corresponding pore size distribution curves of the different carbon samples are shown in Fig. 4. The adsorption capacities of all the samples below the relative pressure (P/P_0) of 0.1 exhibited curves indicating a typical microporous characteristic. Meanwhile, the hysteresis loop at the relative pressure (P/P_0) of 0.4 to 0.95 is associated with the capillary condensation that occurs in the mesopores (Riachy *et al.* 2017). Carbon exhibited a type-I sorption isotherm of microporous characteristic, but the adsorption capacities are obviously low, which exhibits a porosity that is relatively poor for carbon. The C-Zn showed a type-I sorption isotherm. The higher adsorption capacity below the relative pressure (P/P_0) of 0.1 for this sample is due to the increase in micropores (Tian *et al.* 2017). This finding indicates that the presence of $ZnCl_2$ affected mainly the generation of micropores (Erdem *et al.* 2016). The enhanced adsorption capacity for the C-Zn is due to an increase in the contact area between the raw material and the activating agent. The $ZnCl_2$ worked as a dehydration regent during carbonization, endowing the carbon materials with a porous structure and producing a high surface area by removing the hydrogen and oxygen (H_2O) from the feedstock, and leaving behind much more of the elemental carbon (Zhao *et al.* 2017). The adsorption property was obviously improved by using $ZnCl_2$ and NaCl simultaneously as processing agents, which indicates that the synergistic effect of $ZnCl_2$ and NaCl could enhanced the adsorption ability of as-prepared carbon materials. When the ratio of $ZnCl_2$ is dominant, a quantity adsorption of the C-2 was improved upon in comparison to the C-1 below the relative pressure (P/P_0) of 0.1. This observation is probably due to the contraction of pore structure caused by the thermal breakdown of the corncob skeleton under the high ratio of the activating agent ($ZnCl_2$) to the carbon precursor. When the ratio of $NaCl_2$ was dominant, a hysteresis loop in the C-0.5 was enhanced in comparison to the C-1 at the relative pressure (P/P_0) of 0.4 to 0.95. Further, when the NaCl agent was a single agent, the quantity adsorption saw a significant decrease. These results explain that the as-prepared C-Zn mainly showed microporous structure, and the C-Na exhibited mesopores structure. Moreover, eutectic salts were more favorable to the formation of pores than single salt, which could be attributed to the increase in the activating agent enhancing the thermal decomposition rate of the feedstock, and therefore, increasing the surface area of the as-prepared carbon.

The pore size distribution plots of the as-prepared samples are shown in Fig. 4b. The carbon exhibits a uniform pore size distribution, and its pore size mainly distributes in the range of 1.8 nm to 2.5 nm, with a peak at 2.0 nm. The as-prepared C-Zn displays an analogous pore size distribution and peak position to the carbon sample, but a higher peak occurred at 2.0 nm for more of the micropores. An intense and sharp peak of the C-2 appeared at 2.0 nm, indicating a uniform pore size distribution. However, with the increase of NaCl in the eutectic salt system, a larger number of mesopores were generated, while the number of microspores decreased for the C-1 and C-0.5, leading to a wider pore size distribution. Additionally, the C-Na exhibited a similar pore size distribution plot to the carbon except for the peak migration and the width of the pore size distribution. Obviously, the C-Na had a pore size distribution from 2.0 nm to 4.0 nm and the peak appeared at 2.8 nm, which indicates that larger mesopores were generated in the sample of C-Na than the carbon. The results show that the type and amount of porogens are an important influencing factor on the textural properties of the resultant carbon materials (Zhao *et al.*2017). Therefore, the pore size of the as-prepared carbon materials can be controlled by adjusting the ratio of the $ZnCl_2$/NaCl in the eutectic salt system. The use of $ZnCl_2$ independently promoted the formation of micropores and had little effect on the mesopores, *i.e.*, in the as-prepared C-Zn. The addition of NaCl within a certain extent further facilitated the generation of micropores, i.e. in the as-prepared sample, C-2. Nevertheless, this trend was reversed with the increase of NaCl in the eutectic salt system, which resulted in reduced micropores and an increase in the mesopores of the as-prepared samples C-1 and C-0.5. The phase separation of the newly formed carbon materials and the $ZnCl_2$/NaCl ratio may lead to the formation of pores in the carbon materials, which are dominated by mesopores and micropores. These findings indicate that NaCl played a role as the template for mesopores, and $ZnCl_2$ works as an activation agent for micropores.

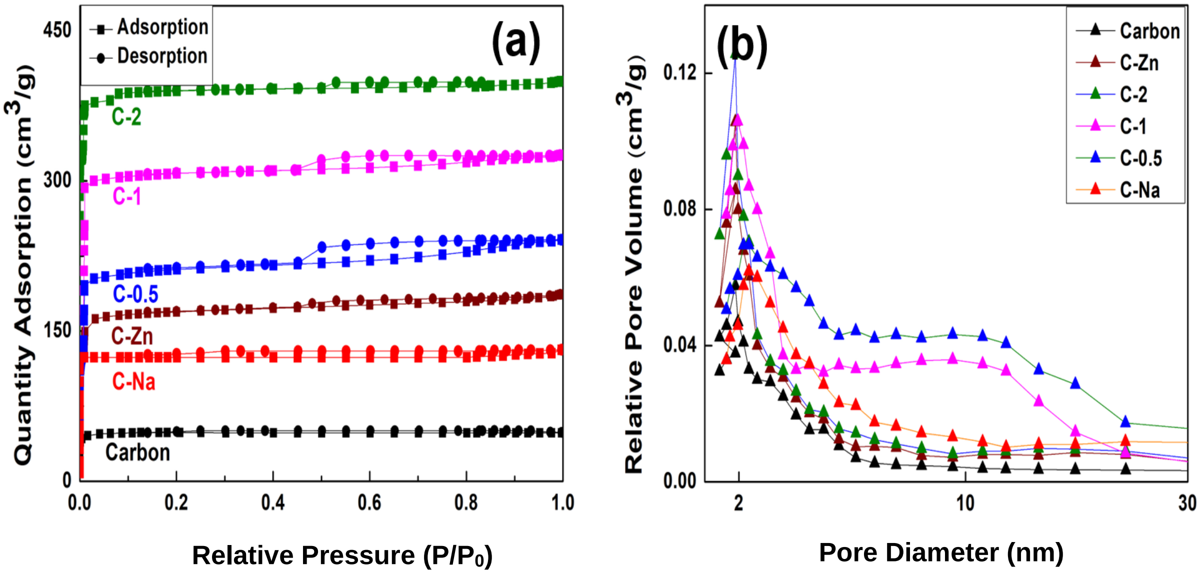

Fig. 4. Nitrogen sorption isotherms (a) and pore size distribution plots (b) of the as-prepared carbon samples

Textural parameters of different carbon samples are listed in Table. 1. Carbon showcased a low specific surface area (130 m^2/g) and pore volume (0.07 cm^3/g), and the pore structure is dominated by micropores (S_{micro}/S_{BET} = 80%). The higher specific surface areas (360 m^2/g, 289 m^2/g) and pore volumes (0.12 cm^3/g, 0.10 cm^3/g) of the C-Zn and C-Na are shown, but the S_{micro}/S_{BET} increased to 87%, and decreased to 68% in each, respectively. The above results suggest that both of $ZnCl_2$ and NaCl have important roles in controlling the surface area and porous percentage of resultant carbons. That is, the NaCl plays a crucial role in the formation of mesopores, and similarly the effects of $ZnCl_2$ is to promote the generation of micropores that result in a larger surface area. Furthermore, the amount of $ZnCl_2$ also affected the S_{BET} of the as-prepared samples when the eutectic salt $ZnCl_2$/NaCl was used in the production of the carbon materials. The S_{BET} increased from 582 m^2/g in the C-0.5 to 762 m^2/g in the C-1 sample, and then further reached 960 m^2/g in the C-2 sample as the amount of $ZnCl_2$ in eutectic salt system increased. This finding is attributed to the role of $ZnCl_2$ in increasing the number of micropores. Moreover, the average pore size decreased from 3.1 nm in the C-0.5 to 2.0 nm in the C-2, which provided further evidence of the function of $ZnCl_2$ in the shrinkage of the pore size. As can be seen, the nitrogen adsorption capacities of as-prepared carbon materials derived from salt solution are clearly higher than those derived from precursors. And the synergistic effect of eutectic salt $ZnCl_2$/NaCl could control the structure of the pores, pore size, and surface area. In particular, the high surface area of the material exposes the more active centers to the reactants, and an appropriate pore volume can improve the adsorption and diffusion of the reactant molecules (Liu and Antonietti 2014).

Table 1. Textural Parameters of Different Carbon Samples

Sample	S_{BET} (m^2/g)	S_{meso} (m^2/g)	S_{micro} (m^2/g)	V_{total} (cm^3/g)	Average pore size (nm)
Carbon	130	32	98	0.07	2.3
C-Zn	360	47	313	0.12	1.8
C-2	960	160	800	0.31	2.0
C-1	762	256	533	0.25	2.5
C-0.5	582	224	308	0.17	3.1
C-Na	289	174	115	0.10	3.5

The adsorption isotherms of formaldehyde gas (Fig. 5a) and butyraldehyde gas (Fig. 5b) distributed by the different carbon samples are shown in Fig. 5. The carbons exhibited an excellent adsorption performance for the two tested organic aldehydes.

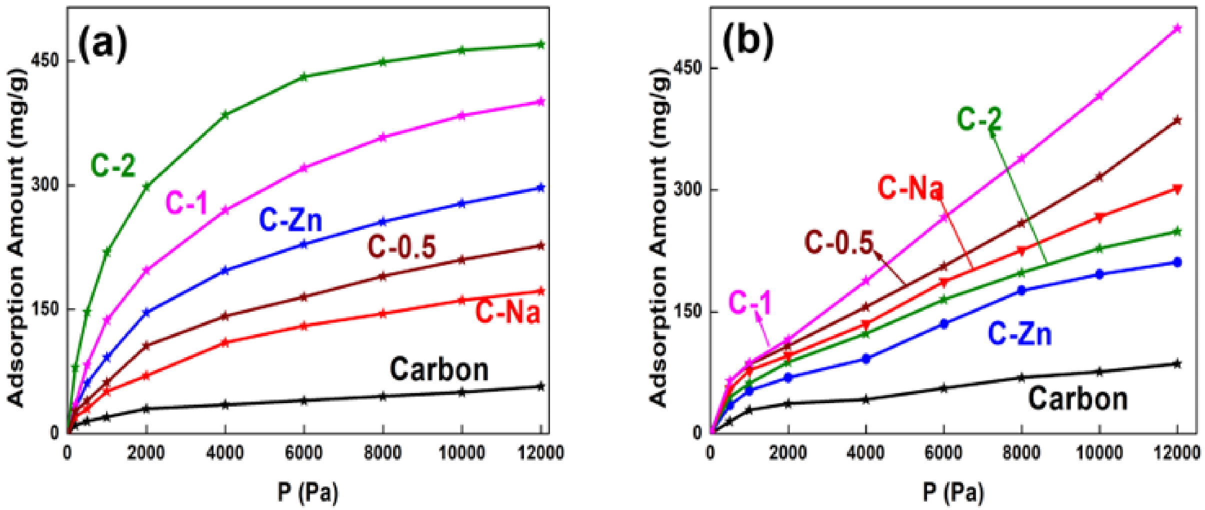

Fig. 5. Adsorption isotherms of formaldehyde gas (a) and butyraldehyde gas (b) by the different carbon samples

The adsorption ability is in the order of C-2>C-1>C-Zn>C-0.5>C-Na>carbon for the formaldehyde gas. The formaldehyde gas adsorption capacity is interrelated with the microporous content of the carbons. This can be attributed to an increase in the microporous specific surface area, which led to more adsorption sites that allowed the formaldehyde gas to be absorbed onto the pore structure quickly and efficiently. The adsorption ability was in the order of C-1>C-0.5>C-Na>C-2>C-Zn>carbon for the butyraldehyde gas. This order is attributed to how the adsorption amount of the butyraldehyde is dependent on the specific surface of the mesopores, as well as how the mesopores can provide a fast diffusion channel and short diffusion distance. During the carbonization of the raw material, $ZnCl_2$ has a skeleton role for the new carbon, leading to placement of the new carbon deposition on it. New carbon has a primary key to adsorption and can thus make the carbon and organic aldehyde stick together (Van *et al.* 2017). The results exhibit that the activity enhancement that occurs with the additions of $ZnCl_2$ may be related to the increase in the surface area. The synergistic effect that occurs from the mixtures leads to a higher specific surface area, further achieving the higher adsorption ability for the organic aldehyde. The high surface area of the carbon materials exposes the more active centers to the reactants, and an appropriate pore volume will improve the diffusion of the reactant molecules, which may serve as the main reasons. The formaldehyde gas adsorption amount of the C-2 and the butyraldehyde gas adsorption amount of the C-1 reach to 460 mg/g and 480 mg/g, respectively.

Figure 6 exhibits the adsorption isotherm for the formaldehyde and butyraldehyde gas of the superior carbon (C-2 and C-1) through the Langmuir and Freundlich model. Superior carbon materials showed the better fitting curve of the Langmuir model, and the coefficients of determination R^2 for the C-2 (0.997) and C-1 (0.982) were closer to 1 (Table 2), indicating a better composite of the Langmuir model for the adsorption process. The value of 1/n is between 0.1 to 0.5 for the formaldehyde gas of the C-2 sample through the Freundlich model and is between 0.5 to 2 for the butyraldehyde gas of the C-1 sample through Freundlich model. The results indicated it easily occurred for the adsorption process, which is a physical adsorption.

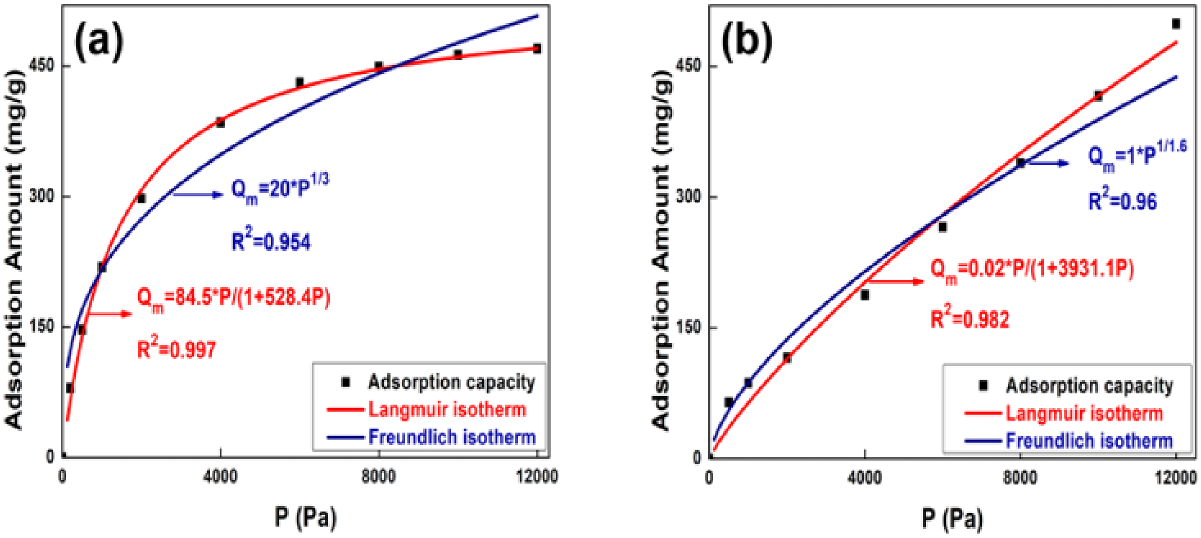

Fig. 6. Formaldehyde gas for the C-2 (a) and the butyraldehyde gas for the C-1 (b) by the Langmuir and Freundlich model isotherm

Table. 2 Summary of the Langmuir Adsorption Parameters of the Formaldehyde and Butyraldehyde on the C-2 and C-1 Samples

Sample	Langmuir			Freundlich		
	a	*b*	R^2	1/n	*K*	R^2
C-2 for Formaldehyde	528.469	8.090	0.997	0.343	20.244	0.954
C-1 for Butyraldehyde	3931.084	4.649	0.982	0.625	1	0.960

a: constant, reflects the adsorption capacity
b: the total adsorption number on 1 cm^2
1/*n*: constant, depends on type of adsorbent, and adsorption temperature
K: constant, depends on type of adsorbent, and adsorption temperature

The adsorption kinetics of the formaldehyde gas for the C-2 and the butyraldehyde gas for the C-1 by pseudo first-order (a) and pseudo second-order (b) are shown in Fig. 7. The pseudo first-order and pseudo second-order (b) dynamic model equations are shown in Eqs. 1 and 2.

$$\ln (q_e - q_t) = \ln q_e - kt \tag{1}$$

$$q_e - q_t = q_e \cdot e^{-kt} \tag{2}$$

$$q_t = q_e (1 - e^{-k_1 t}) \tag{3}$$

$$t/q_m = t \cdot 1/q + 1/k_2 q_e^2 \tag{4}$$

The formaldehyde adsorption reached a stable state during the 120 min to 160 min (Fig. 7a) period. Superior carbon materials showed a slightly better fitting curve for the pseudo first-order, and the coefficients of determination R^2 for the C-2 (0.998) and C-1 (0.999) were closer to 1 (Fig. 7a), indicating that the adsorption followed a pseudo first order kinetic model.

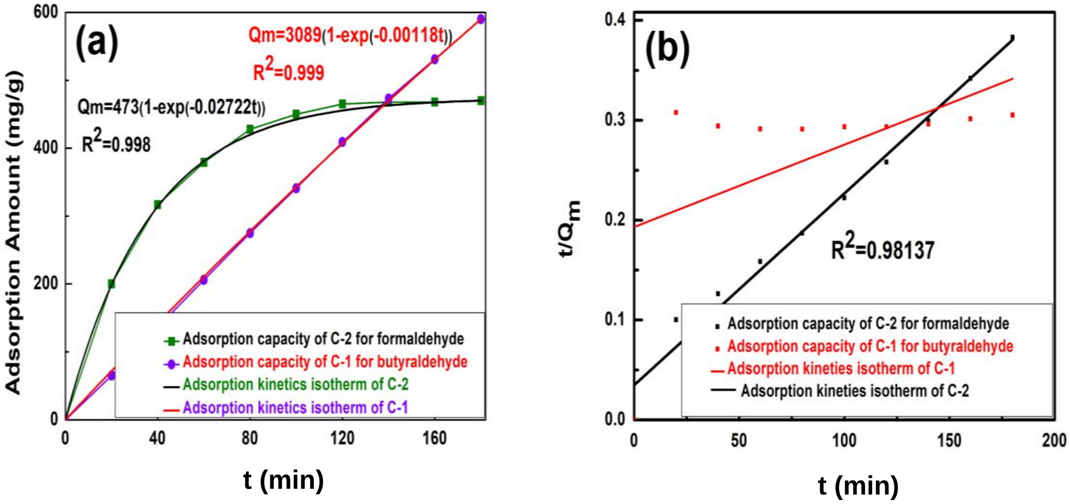

Fig. 7. Adsorption kinetics of the pseudo first-order (a) and pseudo second-order (b) for the adsorption formaldehyde for C-2 (a) and adsorption butyraldehyde for C-1 (b) at different times

The organic aldehyde molecules gradually adsorb onto the carbon surface by adsorption kinetics of the pseudo first-order. The free energy of the adsorption Δ*G* was calculated based on Eq. 5 (Wang *et al.* 2004),

$$K = (1/55.5) \exp(-\Delta G/RT) \quad (5)$$

where ΔG is the free energy of adsorption, K is the adsorption–desorption equilibrium constant, R (J/(mol*K)) is the universal gas constant, and T is the absolute temperature in Kelvins (K).

The values of ΔG were 15.14 kJ/mol and 13.76 kJ/mol for the adsorption formaldehyde for C-2 and the adsorption butyraldehyde for C-1, respectively. Systems having an energy of adsorption in the neighborhood of 20 kJ/mol are generally regarded as physical adsorption (Abu *et al.* 2016). The results showed good agreement to the Langmuir isotherm model. The adsorption kinetics fit very well to both pseudo-first-order rate equation and to a pseudo-second order rate equation.

CONCLUSIONS

1. The morphologies and textural of carbon are highly dependent on the ratio of the eutectic salt $ZnCl_2$/NaCl from the corncob waste. The change in the morphology of the interconnected macropores is attributed to the combination of inherent pores in the cellular structures of the corn husks with different eutectic salt.
2. NaCl plays a crucial role in the formation of mesopores in the resultant carbons, and a series of carbon materials with a high surface area are obtained by the addition of $ZnCl_2$. In particular, the synergistic effect of the eutectic salt $ZnCl_2$/NaCl is seen on the controlled porous structures and pore size. The mesopores can provide a fast diffusion channel and short diffusion distance, and the micropores can enhance adsorption ability for the organic aldehyde.
3. The adsorption ability is in the order of C-2>C-1>C-Zn>C-0.5>C-Na>carbon and C-1>C-0.5>C-Na>C-2>C-Zn>carbon for the formaldehyde and butyraldehyde gas, respectively. This finding is attributed to how the adsorption amount of the formaldehyde and butyraldehyde are dependent on the specific surface of the microporous and mesopores, respectively.
4. The organic aldehyde molecules gradually adsorbed onto the carbon surface through adsorption kinetics consistent with either a pseudo first-order or pseudo-second-order rate. The values of ΔG were 15.14 kJ/mol and 13.76 kJ/mol for the adsorption formaldehyde of the C-2 and the adsorption butyraldehyde of C-1, respectively. The adsorption mode belonging to the physical adsorption, with a ΔG value of approximately 20 kJ/mol.

ACKNOWLEDGMENTS

The present work was financially supported by The National Natural Science Foundation of China (Grant No. 31800499, 31600472, 31570566), The Natural Science Foundation of Shandong (ZR2017LEM009, ZR2016YL007), The Joint Research Fund for young doctor of Qilu University of Technology (Shandong Academy of Sciences) (No. 2017BSH2010), The Key Research and Development Program of Shandong Province (No. 2017GSF17130), The Foundation of Guangxi Key Laboratory of Clean Pulp & Papermaking and Pollution Control of China (KF201717), and The Foundation of Key Laboratory of Pulp and Paper Science and Technology of Ministry of Education/Shandong Province of China (No. ZR201707, No. ZR201710).

Conflicts of Interest

The authors declare no conflict of interest.

REFERENCES CITED

Abu, D., Muna, A., Nathir, A. F., and Mutlaq, A. A. (2016). "Green approach to corrosion inhibition of mild steel by lignin sulfonate in acidic media," *J. of Iron and Steel Research International* 23(7), 722-732. DOI: 10.1016/S1006-706X(16)30112-1

Chen, M., Wang, J., Jiang, B., and Yang, Y. (2012). "Diffusion measurements of isopentane, 1-hexene, cyclohexane in polyethylene particles by the intelligent gravimetric analyzer," *Journal of Applied Polymer Science* 127(2), 1098-1104. DOI:10.1002/app.37948

Erdem, M., Orhan, R., and Şahin, M. (2016). "Preparation and characterization of a novel activated carbon from vine shoots by $ZnCl_2$ activation and investigation of its rifampicine removal capability," *Water, Air, and Soil Pollution* 227(7), 1-14. DOI: 10.1007/s11270-016-2929-5

Falco, G., Li, W. L., Cimino, S., and Bandosz, T. (2018). "Role of sulfur and nitrogen surface groups in adsorption of formaldehyde on nanoporous carbons," *Carbon* 138, 283-291. DOI: 10.1016/j.carbon.2018.05.067

Fellinger, T. P., Thomas, A., and Yuan, J. (2013). "25th anniversary article: Cooking carbon with salt: Carbon materials and carbonaceous frameworks from ionic liquids and poly (ionic liquid)," *Adv. Mater.* 25(41), 5838-5855. DOI: 10.1002/adma.201301975

Fuchs, I., Fechler, N., and Antonietti, M. (2016). "Enantioselective nanoporous carbon based on chiral ionic liquids," *Angew. Chem. Int. Edit.* 55(1), 408-412. DOI: 10.1002/anie.201505922

Gao, S., Chen, Y., Fan, H., Wei, X., and Qu, L. (2014). "Large scale production of biomass-derived N-doped porous carbon spheres for oxygen reduction and supercapacitors," *J. Mater. Chem. A.* 2(10), 3317-3324. DOI: 10.1039/c3ta14281g

Han, J., Zhang, L., Zhao, B., Qin, L. B., Wang, Y., and Xing, F. T. (2019). "The N-doped activated carbon derived from sugarcane bagasse for CO_2 adsorption," *Ind. Crop. Prod.* 128, 290-297. DOI: 10.1016/j.indcrop.2018.11.028

Hattori, Y., Kojima, R., and Sagisaka, K. (2017). "Preparation and formation mechanism of porous carbon nanosheets by thermal decomposition of polyvinyl alcohol films impregnated with zinc (II) and nitrate ions," *Solid. State Sci.* 65, 33-40. DOI:

10.1016/j.solidstatesciences.2017.01.002

He, X., Ling, P., and Qiu, J. (2013). “Efficient preparation of biomass-based mesoporous carbons for supercapacitors with both high energy density and high-power density,” *J. Power Sources* 240, 109-113. DOI: 10.1016/j.jpowsour.2013.03.174

Jiang, Q., Zhang, Z. H., Yin, S. Y., Guo, Z. P., and Wang, S. Q. (2016) “Biomass carbon micro/nano-structures derived from ramie fibers and corncobs as anode materials for lithium-ion and sodium-ion batteries,” *Appl. Surf. Sci.* 379, 73-82. DOI: 10.1016/j.apsusc.2016.03.204

Kante, K., Florent, M., Temirgaliyeva, A., Lesbayev, B., and Bandosz, T. J. (2019). “Exploring resistance changes of porous carbon upon physical adsorption of VOCs,” *Carbon* 146, 568-571. DOI: 10.1016/j.carbon.2019.02.039

Karnan, M., Subramani, K., and Srividhya, P. K. (2017) “Electrochemical studies on corncob derived activated porous carbon for supercapacitors application in aqueous and non-aqueous electrolytes,” *Electrochim. Acta* 228, 586-596. DOI: 10.1016/j.electacta.2017.01.095

Kim, D., and Jeon, J. (2015). “Study on durability and stability of an aqueous electrolyte solution for zinc bromide hybrid flow batteries,” *Journal of Physics: Conference. Series. IOP. Publishing. 574 (1)*, 012074. DOI: 10.1088/1742-6596/574/1/012074

Liu, F. F., Peng, H. L., Qiao, X. C., Fu, Z. Y., and Huang, P. Y. (2017). “High-performance doped carbon electrocatalyst derived from soybean biomass and promoted by zinc chloride,” *Int. J. Hydrogen Energ.* 39(19), 10128-10134. DOI: 10.1016/j.ijhydene.2014.04.176

Liu, X. F., and Antonietti, M. (2014). “Molten salt activation for synthesis of porous carbon nanostructures and carbon sheets,” *Carbon* 69, 460-466. DOI: 10.1016/j.carbon.2013.12.049

Ma, Z. S., Zhang, H. Y., Yang, Z. Z., Zhang, Y. F., and Liu, Z. M. (2014) “Highly mesoporous carbons derived from biomass feedstocks templated with eutectic salt $ZnCl_2$/KCl,” *J Mater Chem A.* 2(45), 19324-19329. DOI: 10.1039/C4TA03829K

Riachy, P., Lopez, G., and Emo, M. (2017). “Investigation of a novel fluorinated surfactant-based system for the design of spherical wormhole-like mesoporous silica,” *J. Colloid Interf. Sci.* 487, 310-319. DOI: 10.1016/j.jcis.2016.10.053

Spagnoli, A. A., Giannakoudakis, D. A., and Bashkova, S. (2017). “Adsorption of methylene blue on cashew nut shell based carbons activated with zinc chloride: The role of surface and structural parameters,” *J. Mol. Liq.* 229, 465-471. DOI: 10.1016/j.molliq.2016.12.106

Tian, X., Ma, H., and Li, Z. (2017). “Flute type micropores activated carbon from cotton stalk for high performance supercapacitors,” *J. Power Sources* 359, 88-96. DOI: 10.1016/j.jpowsour.2017.05.054

Valentín-Reyes, J., García-Reyes, R. B., García-González, A., Soto-Regalado, E., and Cerino-Córdova, F. (2019). “Adsorption mechanisms of hexavalent chromium from aqueous solutions on modified activated carbons,” *J. Environ. Manage.* 236, 815-822. DOI: 10.1016/j.jenvman.2019.02.014

Van, T. T., Bui, Q. T. P., and Nguyen, T. D. (2017). “A comparative study on the removal efficiency of metal ions (Cu^{2+}, Ni^{2+}, and Pb^{2+}) using sugarcane bagasse-derived $ZnCl_2$-activated carbon by the response surface methodology,” *Adsorpt. Sci. and Technol*. 35(1-2), 72-85. DOI: org/10.1177/0263617416669152

Wang, H. L., Liu, R. B., and Xin, J. (2004). “Inhibiting effects of some mercapto-triazole derivatives on the corrosion of mild steel in 1.0 M HCl medium,” *Corrosion Science*

46(10), 2455-2466. DOI: 10.1016/j.corsci.2004.01.023

Yek, P. N. Y., Liew, R. K., Osman, M. S., Lee, C. L., Chuah, J. H., Park, Y. K., and Lam, S. S. (2019). "Microwave steam activation, an innovative pyrolysis approach to convert waste palm shell into highly microporous activated carbon," *J. Environ. Manage.* 236, 245-253. DOI: 10.1016/j.jenvman.2019.01.010

Zhao, S., Yan, T., and Wang, Z. (2017). "Removal of NaCl from saltwater solutions using micro/mesoporous carbon sheets derived from watermelon peel *via* deionization capacitors," *RSC Advances.* 7(8), 4297-4305. DOI: 10.1039/c6ra27127h

Zhao, X., Chen, H. L., Kong, F. G., Zhang, Y. J., Wang, S. J., Liu, S. X., Lucia, L. A., Fatehi, P., and Pang, H. (2019). "Fabrication, characteristics and applications of carbon materials with different morphologies and porous structures produced from wood liquefaction: A review," *Chem. Eng. J.* 364, 226-243. DOI: 10.1016/j.cej.2019.01.159

Zhu, L. H., Gao, Q. M., Tan, Y. L., Tian, W. Q., Xu, J. D., Yang, K., and Yang, C. X. (2015). "Nitrogen and oxygen co-doped microporous carbons derived from the leaves of Euonymus japonicas as high performance supercapacitor electrode material," *Microporous. Mesoporous. Mat.* 210, 1-9. DOI: 10.1016/j.micromeso.2015.02.014

Article submitted: June 12, 2019; Peer review completed: August 15, 2019; Revised version received and accepted: August 26, 2019; Published: September 23, 2019.
DOI: 10.15376/biores.14.4.8835-8848